Effect of post annealing on the band gap of $Mg_xZn_{1-x}O$ thin films

2008 Semicond. Sci. Technol. 23 035002

(http://iopscience.iop.org/0268-1242/23/3/035002)

Semicond. Sci. Technol. **23** (2008) 035002 (5pp) doi:10.1088/0268-1242/23/3/035002

Effect of post annealing on the band gap of $Mg_xZn_{1-x}O$ thin films

D Y Jiang[1,2], D Z Shen[1], K W Liu[1,2], C X Shan[1], Y M Zhao[1,2], T Yang[1], B Yao[1], Y M Lu[1] and J Y Zhang[1]

[1] Key Laboratory of Excited State Processes, Changchun Institute of Optics, Fine Mechanics and Physics. Chinese Academy of Sciences. 16-Dongnanhu Road, Changchun 130033, People's Republic of China
[2] Graduate School of the Chinese Academy of Science, People's Republic of China

Received 7 October 2007, in final form 19 December 2007
Published 25 January 2008
Online at stacks.iop.org/SST/23/035002

Abstract

In this work, $Mg_xZn_{1-x}O$ (MZO) thin films were grown on quartz by rf magnetron sputtering technology. It was found that MZO films possess preferred *c*-axis orientation and exhibit hexagonal wurtzite structure up to a Mg composition of 44.26 mol%. Furthermore, the band gap determined by absorption spectra was smaller than the theoretical calculation for the as-grown MZO thin film. The band gap blueshifted initially and then redshifted with increasing the annealing temperature of the MZO films. The reason for the shift was attributed to the displacement, effusion of Mg atoms in the films and phase separation at different annealing temperatures.

(Some figures in this article are in colour only in the electronic version)

1. Introduction

ZnO has long been treated as one of the strongest candidates for ultraviolet (UV) light-emitting diodes (LED) and laser diodes (LD) due to its wide band gap of 3.37 eV and large exciton binding energy of 60 meV at room temperature [1]. The alloyed $Mg_xZn_{1-x}O$ has been considered as a suitable barrier layer for ZnO LD [2] and has great potential applications in a solar-blind ultraviolet (UV) detector [3]. Due to the very small difference in the ionic radius of Mg^{2+} (0.57 Å) and Zn^{2+} (0.60 Å) [4], relative little lattice distortion can be caused if Zn is replaced by Mg although the band gap can be changed greatly.

Up to now, a variety of techniques have been employed to deposit high quality MZO films, such as pulsed laser deposition (PLD) [5], molecular beam epitaxy (MBE) and rf magnetron co-sputtering [6, 7]. However, due to the different crystal structures of ZnO (wurzite) and MgO (NaCl-type), the solubility limit of Mg in ZnO films while keeping the wurtzite structure is very confined. The limit is found to depend on the deposition technique used and the processing conditions employed. Deposition techniques such as PLD have shown a solubility limit of 33% of Mg in ZnO [5], but the MZO films grown by MOVPE and co-sputtering have shown enhanced solubilities of 49 and 46%, respectively [8, 9]. It is interesting to note that in wurtzite MZO films grown by PLD and sputtering showed a similar band gap variation (for $x \leqslant 0.33$), but when the Mg composition was about 0.45, the films showed a slightly larger band gap (4.94 eV) in comparison to the sputtering films (4.21–4.27 eV).

In the present work, the wurtzite MZO thin films with the Mg content of 44.26% are prepared by using the rf magnetron sputtering technique. The effect of post annealing on the band gap of the MZO thin films was studied. The reason for the experimental band gap being lower than the theoretical results in MZO thin films was discussed.

2. Experiments

An $Mg_{0.45}Zn_{0.55}O$ target was prepared by sintering the mixture of MgO (99.99%) and ZnO (99.99%) powders at 1273 K for 10 h in air ambient. The quartz substrate was cleaned sequently in an ultrasonic bath with acetone, ethanol and de-ionized water at room temperature. The sputtering chamber was evacuated to a base pressure of about 3×10^{-4} Pa. The substrate–target distance was maintained at 60 mm. Ultrapure (5 N) Ar gas was introduced into the sputtering chamber through a set of mass flow controller with the flow rate of 45 sccm. The working pressure in the chamber was kept at 1.0 Pa during the film growth, and the temperature at 723 K. The as-grown film was cut into smaller pieces and

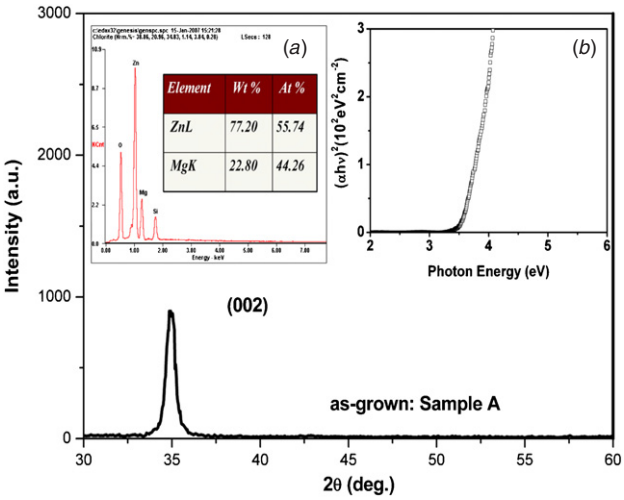

Figure 1. XRD pattern of the as-grown sample A. The insets (*a*) and (*b*) are EDS spectra and the squared absorption coefficient plot of MZO film as a function of photon energy, respectively.

transferred into a tube furnace for annealing. The samples were annealed at 823, 923, 1023 and 1123 K for 30 min in an oxygen flux of 3 l min^{-1}.

X-ray diffraction (XRD) spectra were collected with a D/max-RA x-ray spectrometer (Rigaku International Corp., Japan) with Cu Kα radiation of 1.543 Å to obtain the structural information of the films. Hatachi S 4800 energy dispersive spectroscopy (EDS) was used to determine the Mg/Zn ratio in the films. The acceleration voltage and the magnification of EDS were 10 kV and 5000, respectively. Optical transmission and absorption spectra were recorded using a Shimadzu UV-3101 PC scanning spectrophotometer. To investigate the effect of the annealing temperature on the vibration modes, Raman spectra were obtained using the 325 nm line of a He–Cd laser under the back-scattering configuration.

3. Results and discussion

Figure 1 shows the XRD pattern of the as-grown film which is defined as sample A. Only the MZO (0 0 2) peak is observed, which indicates that the MZO thin film keeps the wurtzite structure, and phase separation is not observed. There is 0.6° shift of (0 0 2) peak position in comparison with bulk ZnO, which shows a large Mg content in the MZO film. In general, MZO with a content of Mg larger than 4% is not thermodynamically stable. However, it has been indicated that the solubility limit of Mg in ZnO depends on growth mechanisms as well as the growth conditions employed [10]. Energy dispersive spectroscopy (EDS) was used to determine the Mg/Zn ratio in the MZO thin films. The mole composition of elements of sample A is shown in the inset (a) of figure 1. No other impurities were detected within the detection limit of EDS (~0.5 wt%), and the Mg/Zn ratio is 44.26/55.74 which is very close to the proportion of Mg and Zn in the target. It is opposite to that reported by Yang *et al* [3], who noted that the higher substrate temperature is seen to result in a poor control of the Mg content in the growing MZO film.

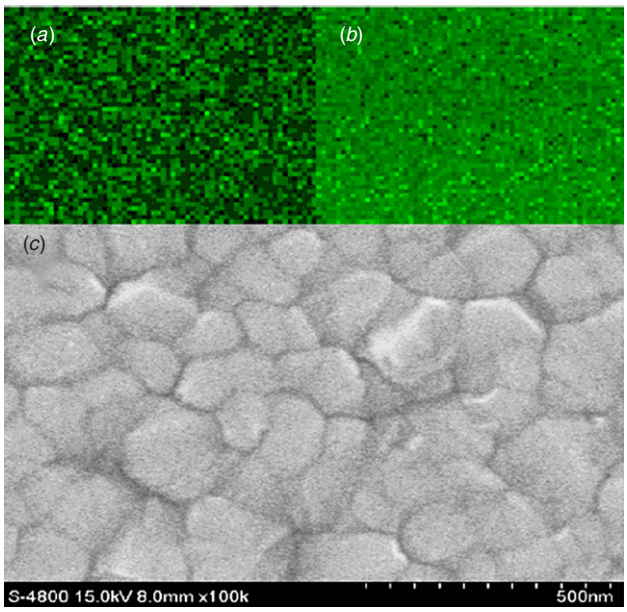

Figure 2. The images of mapscan: (*a*) sample A, (*b*) sample B and (*c*) the SEM of sample A.

The inset (*b*) of figure 1 shows the squared absorption coefficient (α^2) plot of sample A as a function of photon energy according to the following formula [11]:

$$\alpha^2 = (A/h\upsilon)^2(h\upsilon - E_g), \tag{1}$$

where α is the absorption coefficient, A is a constant and $h\upsilon$ is the photon energy. The band gap energy (E_g) can be obtained by plotting $(\alpha h\upsilon)^2$ versus $h\upsilon$ and the linear extrapolation to $\alpha = 0$. The band gap was calculated to be about 3.8 eV. Another way to obtain the band gap of the MZO films is by using the following equation [12]:

$$\mathrm{E}_g(\mathrm{MZO}) = 2.51x + 3.37 \text{ eV} \tag{2}$$

where x is the Mg composition in ZnO. The relationship on band gap energy at room temperature is roughly consistent with Vegard's law (E_g of pseudo-wurtzite MgO at 0 K is calculated to be 6.06 eV theoretically) and can be evidence of the single wurtzite phase. In this way, the band gap obtained is 4.48 eV given that the Mg composition in the film is 44.26%. It has to be noted that there is a huge difference between the band gap values obtained in the two ways. The difference may be attributed to the random distribution of the Mg content in the ternary MZO films, for example, Mg maybe incorporated at the interstitial sites and the grain boundaries. In order to verify our viewpoint, the samples were annealed at 873, 973, 1073 and 1173 K, and the annealed samples were referred to samples B, C, D and E, respectively.

In order to study the spatial distribution of Mg composition, EDS-mapscan images of samples A and B are measured, as shown in figures 2(*a*) and (*b*). The mapscan images have the same scanning size of 1500 × 1500 nm^2, and the dead times are both about 23 s. The resolution ratio was 64 × 50. The mosaic points in the image reveal the Mg composition. The mosaic points were brighter, the Mg

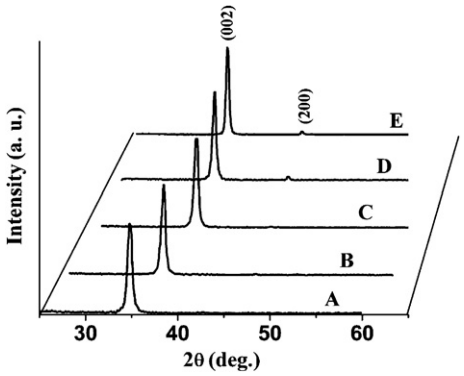

Figure 3. XRD spectra of the as-grown sample A and the samples B, C, D and E annealed at temperatures of 873, 973, 1073 and 1173 K, respectively.

composition was higher and it showed lower Mg composition on the opposite. As shown in figure 2(*a*), there were many brighter and darker nonuniform mosaic points with the size about 23 nm × 30 nm. In comparison with the grain size (100–200 nm, as shown in figure 2(*c*)), it was demonstrated that partial of element Mg was not in lattice points, instead of locating at interstitial sites and the grain boundaries. This can explain the phenomenon of the lower band gap with the higher Mg content. Combining the images of figures 2(*a*) and (*b*), it is concluded that the annealed MZO films showed rather uniform of element Mg. We note that the mapscan images of samples C, D and E (not shown here) are almost the same as that of sample B. We considered that the element Mg was introduced into the normal lattice points with the increasing annealing temperature.

The XRD patterns shown in figure 3 reveal that all the samples have strong diffraction peaks corresponding to (0 0 2) facet of ZnO, indicating that the samples consist mainly of the hexagonal wurtzite structure. After the sample is annealed at 873 K, in addition to the diffraction peaks from the hexagonal ZnO, no other peaks are observed in samples B and C. The full width at half maximum (FWHM) of sample A (0.483°) was larger than samples B (0.432°) and C (0.423°). The shrinkage in FWHM shows that the crystal quality of an as-grown MZO film has been improved after annealing. However, the higher annealing temperature could not lead to the better crystalline quality, instead, (2 0 0) peak located at 42.75° emerged, which belonged to the cubic phase, implying that phase segregation occurs at higher annealing temperature.

The variation of the *c*-axis lattice constant may provide evidence for the incorporation of Mg incorporation. The *c*-axis constant can be calculated by the following formula [13]:

$$c = \frac{\lambda}{2\sin\theta}\sqrt{\frac{4}{3\left(\frac{a}{c}\right)^2}(h^2 + hk + k^2) + l^2} \qquad (3)$$

where h, k and l are the Miller indices, λ is the wavelength of the x-ray and θ is the Bragg diffraction angle. The dependence of the *c*-axis constant on the annealing temperature is shown in figure 4, in which the *c*-axis value decreases initially then increases. Opposite trend has been observed in the position variation of the (0 0 2) diffraction peak.

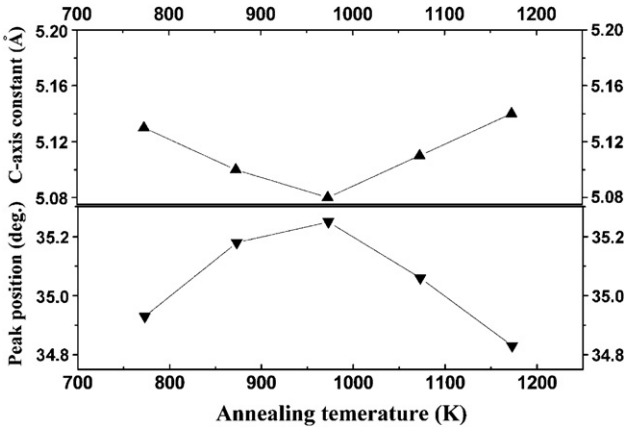

Figure 4. The *c*-axis constant and the dependence of the (0 0 2) peak position of the MZO films on the annealing temperature.

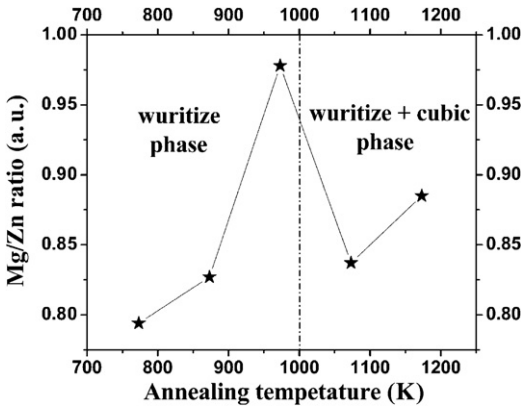

Figure 5. Plot of the Mg/Zn ratio as a function of annealing temperature.

The Mg/Zn ratio as a function of annealing temperature is plotted in figure 5. The ratio increases first, then decreases. It can be concluded that the Mg/Zn ratio depends on the annealing temperature.

Shown in figure 6 is the UV/visible transmittance spectra for the samples. Oscillations are observed in the transmittance spectra, which correspond to multi-reflexions at the film–air and film–substrate interfaces. All samples are highly transparent in the visible region from 400 to 700 nm and have a sharp absorption edge in the UV region. The transmission spectra do not show two absorption edges, which suggests that scattering detect centers remain unaffected with the variation of the Mg content. This result verifies the optical high quality of MZO films. The presence of secondary phase was not clearly seen. This can be correlated with XRD results, which showed the presence of both poor cubic and strong hexagonal phases. It may be proved that all samples mainly keep hexagonal wurtzite structure. The absorption edge shifted to a short wavelength as the ratio of Mg/Zn increased from sample A to sample C, which indicated that the band gap energy of MZO depended on the ratio of Mg/Zn. Furthermore, the crystal quality of sample C was enhanced obviously. But

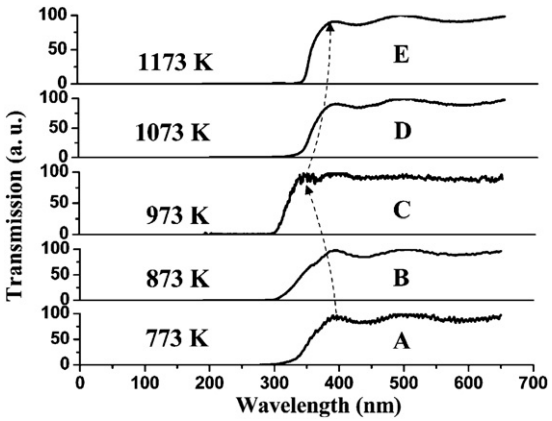

Figure 6. Transmission spectra for sample A and the samples B, C, D and E annealed at different temperatures.

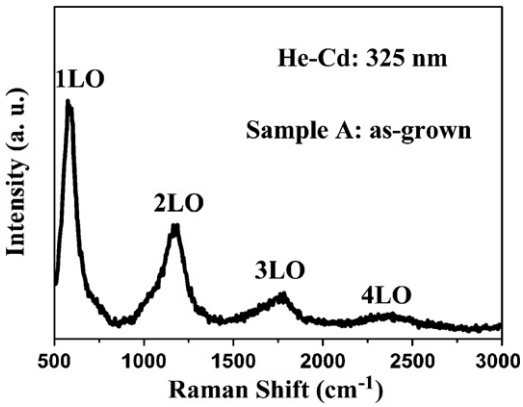

Figure 8. Raman scattering spectrum of the as-grown sample A.

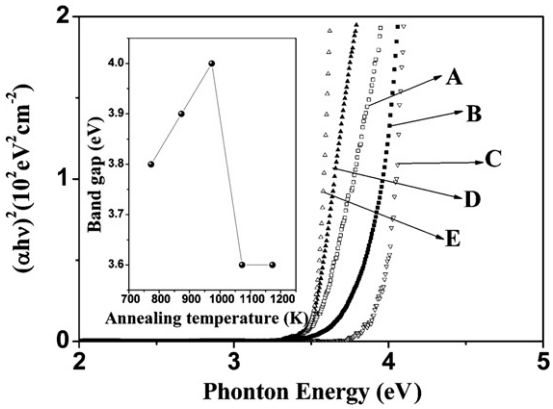

Figure 7. The squared absorption coefficient plots of all samples as a function of photon energy. The inset shows the relationship between the band gap and annealing temperature.

from sample C to sample E, the absorption edge shifted to the other side. This variation trend can be seen clearly in figure 7.

Figure 7 shows the squared absorption coefficient plots of all samples as a function of photon energy. The inset of figure 7 shows the relationship between the band gap and annealing temperature. By using the calculated equation of band gap and linear extrapolation, the band gaps of samples A–E are calculated to be 3.8, 3.9, 4.0, 3.6, 3.6 eV, respectively, which are larger than those of ZnO bulk or thin films. As can be seen clearly, the band gap of MZO thin films depended on the annealing temperature, and can be adjusted between 3.6 and 4.0 eV. The band gap shifted to the higher energy side can be attributed to Mg atoms, which are induced to the lattice points. According to the result of SEM measurement, the mean particle size of MZO in this work is larger than 100 nm. Therefore, the quantum confinement effect and the strain cannot be taken into account in these samples. From figure 7, the band gap decreases when the increasing annealing temperature is higher than 923 K. This decrease can be partly attributed to two main reasons. First, it is obviously seen that phase separation will be one of the reasons. Secondly, the same variations of the band gap with different annealing temperature were reported by Ohtomo *et al* who demonstrated that thermal diffusion of Mg starts at 1123 K [14]. This shows some Mg is not at the lattice point. So the bond energy related to Mg was rather poor, which resulted in losing from the thin films of Mg. This is also indirectly confirmed by EDS. Hence, the optical band gap shifted to the lower energy side. This also can explain the variations of the *c*-axis constant.

Raman scattering spectra of the samples are collected in a backscattering geometric configuration at room temperature. All the samples show intense multiphonon scattering in the range from 500 to 3000 cm^{-1}. Figure 8 shows typical resonant Raman scattering spectrum of sample A. The Raman spectrum is composed of four sharp lines at frequency shifts that are multiples of the 1-longitudinal optical (1-LO) zone-center frequency of 587 cm^{-1}. This result is close to previously reported values of the Raman shift for ZnO bulk and thin films [15, 16], which indicates that sample A mainly kept the hexagonal structure. The structures of samples B–F are in good agreement with sample A (not shown here), as confirmed by XRD results. But the intensity of sample F is decreased a little compared with sample A, which is due to the formation of cubic MZO.

The variations of FWHM and the frequency of the 1-LO phonons versus annealing temperature are shown in figure 9. It can be seen from figure 9 that the FWHM of the 1-LO phonons decreases with the increase of the annealing temperature until 923 K, which indicates the improvement of the MZO crystal quality. On the other hand, the element Mg at the interstitial sites and the grain boundaries will be introduced into the normal lattice sites or occupy the Zn sites in the lattice with the increase of the annealing temperature. So the FWHM of the 1-LO phonons which becomes narrower will be attributed to the Mg impurity and intrinsic lattice defects decreasing. But the FWHM of the 1-LO phonons broadened with the annealing temperature from 923 to 1123 K. This indicates that there were some new defects in the lattice. We suggest that some Mg ions are induced by the annealing temperature into the interstitial or the grain

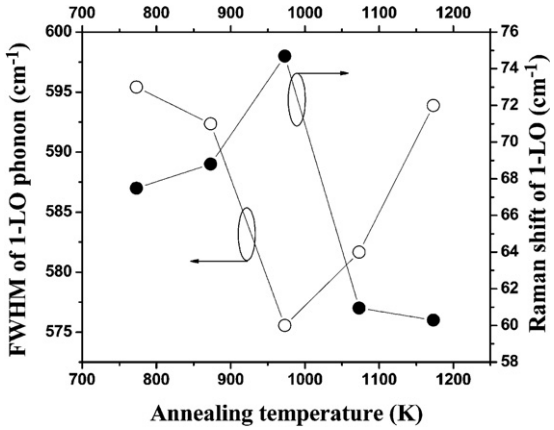

Figure 9. Variations of FWHM (○) and Raman shift (●) of 1-LO phonon with the annealing temperature.

boundaries. With the increasing annealing temperature, the Mg–O bond achieved enough energy, so the Mg–O bond was easily brittle. Hence, some Mg will be lost from the thin films and some Mg will be at the interstitial and grain boundaries. The same conclusion can be conformed by the other hand. The Raman shift of 1-LO phonon was shown the same regularity with the variations of the FWHM of 1-LO phonon. The compressive strain will induce the blue shift of the 1-LO phonon frequencies. But as discussed previously, the strain of the MZO was tensile strain all along, and has a negligible effect on the blue shift of the 1-LO phonon frequencies. Therefore, there may be other mechanisms that affect the frequency dependence of annealing temperature. However, the ion radius of Mg is smaller than Zn, but owing to larger electronegativity. When Mg was introduced into the ZnO lattice, the phonon frequency energy will increase with the increasing annealing temperature. On the opposite side, the red shift of the 1-LO phonon frequencies can be explained by the Mg decrease in the lattice, which is according to the above discussions.

4. Conclusion

In summary, a wurtzite MZO thin film with the Mg concentration of 45 mol% was prepared by rf magnetron sputtering. The distribution of element Mg was nonuniform, as confirmed by the mapscan image. When the annealing temperature was increased from 773 to 973 K, more Mg was incorporated in the lattice sites; as a result, the band gap increases. Hence, the crystal quality of the MZO film was enhanced greatly, which can be confirmed by the variation of sample transmission. But when the annealing temperature was higher than 973 K, phase separation happened. Furthermore, some diffusion Mg (not at lattice point) was easily lost from the film and some new defects were induced. These were the reasons for the red shift of the band gap and the broadening FWHM of 1-LO phonon frequency.

Acknowledgments

This work is supported by the Key Project of the National Natural Science Foundation of China under grant nos 60336020 and 50532050, the Innovation Project of Chinese Academy of Sciences and the National Natural Science Foundation of China under grant nos 60429403, 10674133 and 60506014.

References

[1] Look D C 2001 Recent advances in ZnO materials and devices *Mater. Sci. Eng.* B **80** 383–7
[2] Sun H D, Makino T, Segawa Y, Kawasaki M, Ohtomo A, Tamura K and Koinuma H 2001 Biexciton emission from ZnO/$Zn_{0.74}Mg_{0.26}O$ multiquantum wells *Appl. Phys. Lett.* **78** 3385–7
[3] Yang Y, Hullavard S S, Nagaraj B, Takeuchi I, Sharma R P, Venkatesan T, Vispute R D and Shen H 2003 Compositionally-tuned epitaxial cubic $Mg_xZn_{1-x}O$ on Si(1 0 0) for deep ultraviolet photodetectors *Appl. Phys. Lett.* **82** 3424–6
[4] Zhao D X, Liu Y C, Shen D Z, Lu Y M, Zhang J Y and Fan X W 2002 Structural and optical properties of $Mg_xZn_{1-x}O$ thin films prepared by the sol–gel method *J. Cryst. Growth* **234** 427–30
[5] Ohtomo A, Kawasaki M, Koida T, Masubuchi K, Koinumpa H, Sakurai Y, Yoshida Y, Yasuda T and Segawa Y 1998 $Mg_xZn_{1-x}O$ as a II–VI widegap semiconductor alloy *Appl. Phys. Lett.* **72** 2466–8
[6] Sun H D, Makino T, Segawa Y, Kawasaki M, Ohtomo A, Tamura K and Koinuma H 2002 Enhancement of exciton binding energies in ZnO/ZnMgO multiquantum wells *J. Appl. Phys.* **91** 1993–7
[7] Minemoto T, Negami T, Nishiwaki S, Takakura H and Hamakawa Y 2000 *Thin Solid Films* **372** 173–6
[8] Bhattacharya P, Rasmi R and Katiyar R S 2003 *Appl. Phys. Lett.* **83** 2010–2
[9] Park W I, Yi G-C and Jang H M 2001 Metalorganic vapor-phase epitaxial *Appl. Phys. Lett.* **79** 2022–4
[10] Choopun S, Vispute R D, Yang W, Sharma R P and Venkatesan T 2002 Realization of band gap above 5.0 eV in metastable cubic-phase $Mg_xZn_{1-x}O$ alloy films *Appl. Phys. Lett.* **80** 1529–31
[11] Pawlikowski J M 1982 Absorption edge of Zn_3P_2 *Phys. Rev.* B **26** 4711–3
[12] Koike K, Hama K, Nakashima I, Takada G-Y, Ogata K-I, Sasa S, Inoue M and Yano M 2005 Molecular beam epitaxial growth of wide bandgap ZnMgO alloy films on (1 1 1)-oriented Si substrate toward UV-detector applications *J. Cryst. Growth* **278** 288–92
[13] Li J H, Liu Y C, Shao C L, Zhang X T, Shen D Z, Lu Y M, Zhang J Y and Fan X W 2005 Effects of thermal annealing on the structural and optical properties of $Mg_xZn_{1-x}O$ nanocrystals *J. Colloid Interface Sci.* **283** 513–7
[14] Ohtomo A, Shiroki R, Ohkubo I, Koinuma H and Kawasaki M 1999 Thermal stability of supersaturated $Mg_xZn_{1-x}O$ alloys films and $Mg_xZn_{1-x}O$/ZnO heterointerfaces *Appl. Phys. Lett.* **75** 4088–91
[15] Scott J F 1970 UV resonant Raman scattering in ZnO *Phys. Rev.* B **2** 1209–11
[16] Zhang X T, Liu Y C, Zhang L G, Zhang J Y, Lu Y M, Shen D Z, Xu W, Zhong G Z, Fan X W and Kong X G 2002 Structure and optically pumped lasing from nanocrystalline ZnO thin films prepared by thermal oxidation of ZnS thin films *J. Appl. Phys.* **92** 3293–8